Molecular Insight into the β-sheet Twist and Related Morphology of Self-Assembled Peptide Amphiphile Ribbons

Qinsi Xiong, Samuel I. Stupp, George C. Schatz*

ABSTRACT

Self-assembly of high-aspect-ratio filaments containing β-sheets has attracted much attention due to potential use in bioengineering and biomedicine. However, precisely predicting the assembled morphologies remains a grand challenge because of insufficient understanding of the self-assembly process. We employed an atomistic model to study the self-assembly of peptide amphiphiles (PAs) containing valine−glutamic acid (VE) dimeric repeats. By changing sequence length, the assembly morphology changes from flat ribbon to left-handed twisted ribbon, implying a relationship between β-sheet twist and strength of inter-strand hydrogen bonds. The calculations are used to quantify this relationship including both magnitude and sign of the ribbon twist angle. Interestingly, a change in chirality is observed when we introduce the RGD epitope into the C-terminal of VE repeats, suggesting arginine and glycine's role in suppressing right-handed β-sheet formation. This study provides insight into the relationship between β-sheet twist and self-assembled nanostructures including a possible design rule for PA self-assembly.

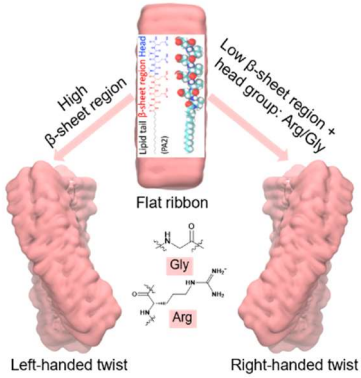

Peptide self-assembly has received significant attention due to outstanding applications of the resulting structures ranging from tissue engineering to drug delivery[1,2]. Peptide amphiphiles (PAs) are an important family of peptide derivatives that have been used for this purpose, and their assembly leads to various self-assembled morphologies, including flat belts[3,4], twisted ribbons[3,5–7], helical ribbons[7], cylinders[8,9], and spherical micelles[10,11]. Of the many PA self-assembly studies, β-sheet formation is found to play a significant role in determining high-aspect-ratio morphologies[12]. Much experimental work has been devoted to exploring the relationship between β-sheet twist and the overall nanostructures. In particular, the self-assembly morphologies can be tuned by changing the sequence length of the β-sheet domains (such as by using a hydrophobic-hydrophilic alternating motif--- VE) [3,4]. Peptides with more hydrophobic side chains have also been shown to increase the lateral stacking of β-sheet structures[13,14]. The distortion of β-sheet tapes can be varied by adjusting the electrostatic interaction between the terminal charges of the peptides, which can cause a different degree of lateral packing of the β-sheets, and ultimately lead to different assembly morphologies[10,15,16].

However, limited by experimental characterization techniques, molecular details of the connection between β-sheet twist and the assembled structures are still obscure. Molecular dynamics simulation can provide a means of exploring these details[17,18], however, most theoretical or computational work has been focused on the assembly of cylindrical micelles[19–21]. A previous work in our group used an all-atom model to simulate the spontaneous twisting of a bilayer C_{18}-$(PEP)_2$ assembly[22]. In that study, Lai and Schatz[22] observed a spontaneous structural transformation from a bilayer ribbon to a left-handed twisted ribbon, and they concluded that residues near the core region tend to form β-sheets while the C- terminus proline-rich region forms PPII conformations. Nevertheless, molecular details on how the β-sheet twist affects chirality remain to be further explored.

Herein, we employed an all-atom model to explore the relationship between β-sheet twist and assembly morphologies. To avoid involving too many non-covalent factors, we chose to model the self-assembly of PAs in an acidic environment, which was also reported in previous experimental work[4]. Therefore, the system considered here involves fully protonated PAs containing a series of simple sequences. Our simulation shows that the morphology changes from flat ribbon to twisted ribbon as the VE repeats increase, which implies a relationship

between β-sheet twist and the strength of inter-strand hydrogen bonds. Moreover, when the RGD epitope is introduced to the head group (C terminal) of peptides, a chiral change from left-handed to right-handed can be observed, therefore suggesting that achiral glycine (Gly) and protonated arginine (Arg) do not contribute to the right-handed twist of the β-sheet when they located in the head region of PA sequence. Overall, this study provides additional understanding of the relationship between β-sheet twist and the resulting self-assembled morphologies, which can be applied to the rational design of PA-based functional nanomaterials.

Three PAs with varied VE dimeric repeats were investigated in the present study to explore the effect of β-sheet content on self-assembled supramolecular structure (Figure 1a). For each PA sequence, we constructed three kinds of bilayer ribbons with different width and length (Table 1, see SI). Previous X-ray diffraction studies of amyloid fibrils suggest that these fibrils are a set of β-sheets that are parallel to the fibril axis, with the hydrogen-bonded-strands perpendicular to this axis[23–25]. However, when it comes to PA ribbon structures, whether the stacked β-sheet is oriented along the width or length direction is still unclear. Therefore, ribbons with hydrogen bonding(H-bonding) oriented along the width (x axis, see Figure S2) and length (y axis, see Figure S3) directions were both considered, choosing $C_{16}(VE)_6$ (hereafter denoted PA3) as the model system. It turns out that ribbons with H-bonding in the length direction do not twist significantly while ribbons with H-bonding along the width direction do twist. Since PA3 has been experimentally confirmed to form twisted nanostructures[3], we decided to simulate ribbons with H-bonding oriented along the width direction for all the PA's. We also considered variations in the PA density, i.e., the interval between PAs (Figure S2c-d), and we found that the ribbon failed to maintain its shape if the density is too low. By using a 4 Å interval in width and 8 Å interval in length as our initial setting, we eventually get an equilibrated ribbon structure with an inter-strand interval of ~4.85 Å and an inter-sheet interval of ~9.95 Å (Figure S4), which matches the experimental results for amyloid fibrils [23–25]. Overall, a 4 Å interval in width and 8 Å interval in length appear to be the most suitable options for producing robust self-assembled twisted ribbon structures.

Table 1. Three kinds of ribbon morphologies with different width and length.

	8^a*10^b PA	8*16 PA	11*16 PA
Width(nm)	3.2	3.2	4.4

Length(nm)	8	12.8	12.8

[a] Number of layers in width
[b] Number of layers in length

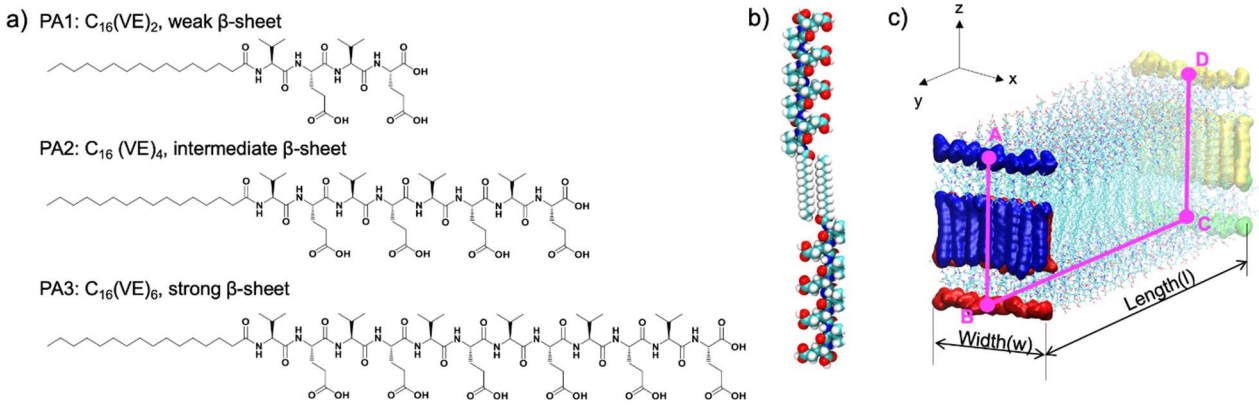

Figure 1. (a) Chemical structures of $C_{16}(VE)_2$, $C_{16}(VE)_4$, and $C_{16}(VE)_6$ PAs. (b) Molecular representation of the peptide amphiphile dimer molecules, here we take $C_{16}(VE)_4$ as an example. (c) Model of self-assembled bilayer ribbon structure used in our simulations. Torsion angle is determined as the dihedral angle in the chain A-B-C-D (highlighted in magenta), which corresponds to the centers of mass of the residues at four edges. Layers directly exposed to the solvent were excluded. So A,B,C,D belongs to the center of mass of inner layer's edge. Distances between each dimer in the x and y directions are 4 and 8 Å, respectively, where the y axis corresponds to the growing axis of the ribbon.

We then performed 100 ns all-atom MD simulations for each PA system and calculated the torsion angle as the dihedral angle between center of mass of the residues at four edges of the ribbon (Figure 1c). To simplify the analysis, we further divided the twisted ribbon into three groups according to the averaged torsion angle(ϒ) for the last 10ns of the production run: Left-hand twist (LH: ϒ<-10º), Flat (F; -10º< ϒ <10º), and Right-hand twist (RH; ϒ > 10º). Interestingly, as the VE repeats increase, the morphology changes from almost flat ribbon (PA1 and PA2) to left-handed twisted ribbon (PA3) (Figure 2). A length or width change in the PA1 or PA2 ribbon doesn't affect the torsion angle much. For PA3, we observed a left-handed twist in the torsion angle range of -10° to -40°, which corresponds to rotation up to 3°/nm along the growing axis. Notably, as the ribbon length increases by a factor of 1.6 (from 8nm to 12.8nm), the torsion angle increases by a factor of 1.5 (from -21º to -41º), while a 37% increase in ribbon width (from 3.2nm to 4.4nm) leads to a 70% decrease of torsion angle (from -41º to -12º), which suggests that the degree of torsion appears to be severely suppressed by lateral growth of the bilayer ribbon nanostructure. Overall, both PA1 and PA2 form flat structures, while PA3 forms

twisted ribbons with a much narrower width, which is in consistent with experimental observations[3].

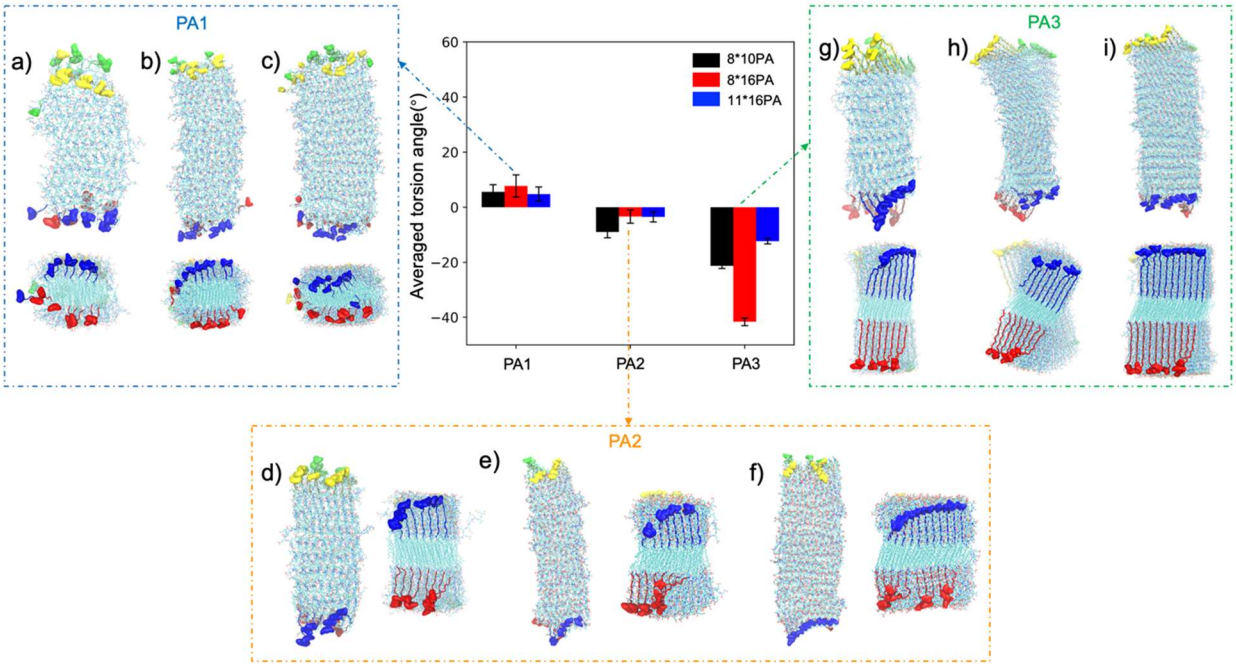

Figure 2. Averaged torsion angle of the PA1, PA2, PA3 ribbons. Snapshots of final simulation structures of PA1(a-c), PA2(d-f), PA3(g-i) ribbons with 8*10 PA, 8*16 PA, and 11*16 PA respectively. Ions and water are omitted for clarity.

We then analyzed the β-sheet content which reflects the hydrogen bond(HB) strength between backbones, and we observed an increase in β-sheet content as the VE dimeric repeats were increased (Figure S5a). Given that peptides with alternating hydrophobic and hydrophilic amino acids have a strong tendency to form β-sheet structures[26–29], this result is predictable. Interestingly, ribbons with the smallest width/length ratio (1:2) have the lowest β-sheet content, suggesting that HB interaction within backbone can be enhanced by the lateral growth of the ribbons. In addition, the distribution of β-sheets along the PA sequence helps to explain the contribution of each amino acid sequence to the overall structure (Figure S5b-d). Except for the last two amino acids, the other residues have a high β-sheet content (50%-80%); the failure of the last two amino acids to form a β-sheet can be explained as arising from strong solvation of the head region of the peptide. Non-bonded interactions within sidechains and a solvation analysis suggest that the PA3 ribbon forms the most stable structure while PA1 is less stable (Figure S6). Considering the results of HB and side chain interactions (Figure S6), we suggest that side-chain interactions are the more dominant interactions in PA1 system. Therefore, more

lateral growth, or even multi-layer accumulation, as suggested by Cui[4], may contribute to the stability of the PA1 ribbon structure. We did not carry out simulations here of these larger structures, due to constraints from size and computational cost.

To gain further insight into the observed correlation between twist of the ribbons and twist of the individual β-strands, we calculated the twist angle distribution within the PA strands (Figure 3a). Such distributions are a well-studied property for isolated β-strands[30]. For the PAs, the distributions of the averaged twist angle are shown in Figure 3b and Figure S7-8, and the results confirm that the PAs have a right-hand twist[30–32]. Meanwhile, the twist angle becomes larger as it gets closer to the PA head group, especially the last angle, which reaches ~50º, suggesting that the chirality of the head group might contribute more to the overall right-handed twist of the peptide[33]. In addition to the right-handed twist of individual strands, the HB formed by the backbone of neighboring PA3 peptides is found to be quite symmetrical and strong (Figure 3c). Individual strands of PA1 and PA2 ribbons also show a right-handed twist of β-strands, but with relatively weak inter-strand H-bonding (Figure S8), sidechain interactions are dominant and eventually lead to flat ribbons. Therefore, our results suggest that although the ribbon twist originates from β-strand twist, a certain amount of inter-strand H-bonding is required to stabilize the ribbon from thermal fluctuations. This is in agreement with the Shamovsky et al. and Wang et al.'s works that while β-sheet twisting is governed by the intrinsic property of intra-strand itself, it is stabilized by stronger inter-strand hydrogen bond interactions[30,34].

To figure out how exactly the twisted β-sheets contribute to the final left-handed twisted ribbons, we further examined the detailed backbone arrangement of the ribbons (Figure 3d). Interestingly, the β-sheets have a right-handed twist along the PA's chain direction (z axis). In terms of the stacking geometry, to form a highly packed and minimal solvent accessible nanostructure, the right-handed β-sheets naturally stack left-handed in the ribbon growth direction (y axis). As a result, a left-handed twisted ribbon is produced. This observation is related to conclusions of previous amyloid fibrils studies where right-handed β-strands produce a left-handed twist in the β-sheet (along the axis normal to the polypeptide chain), resulting in the left-handed fibrils[34,35]. Interestingly, Mezzenga and co-workers found the opposite trend in another study of fibrils, in which a peptide chain with right-handed β-strands formed a right-

handed fibril. However this work found that the fibril twist was induced by the interdigitation of the termini[36], which is an effect that does not apply here.

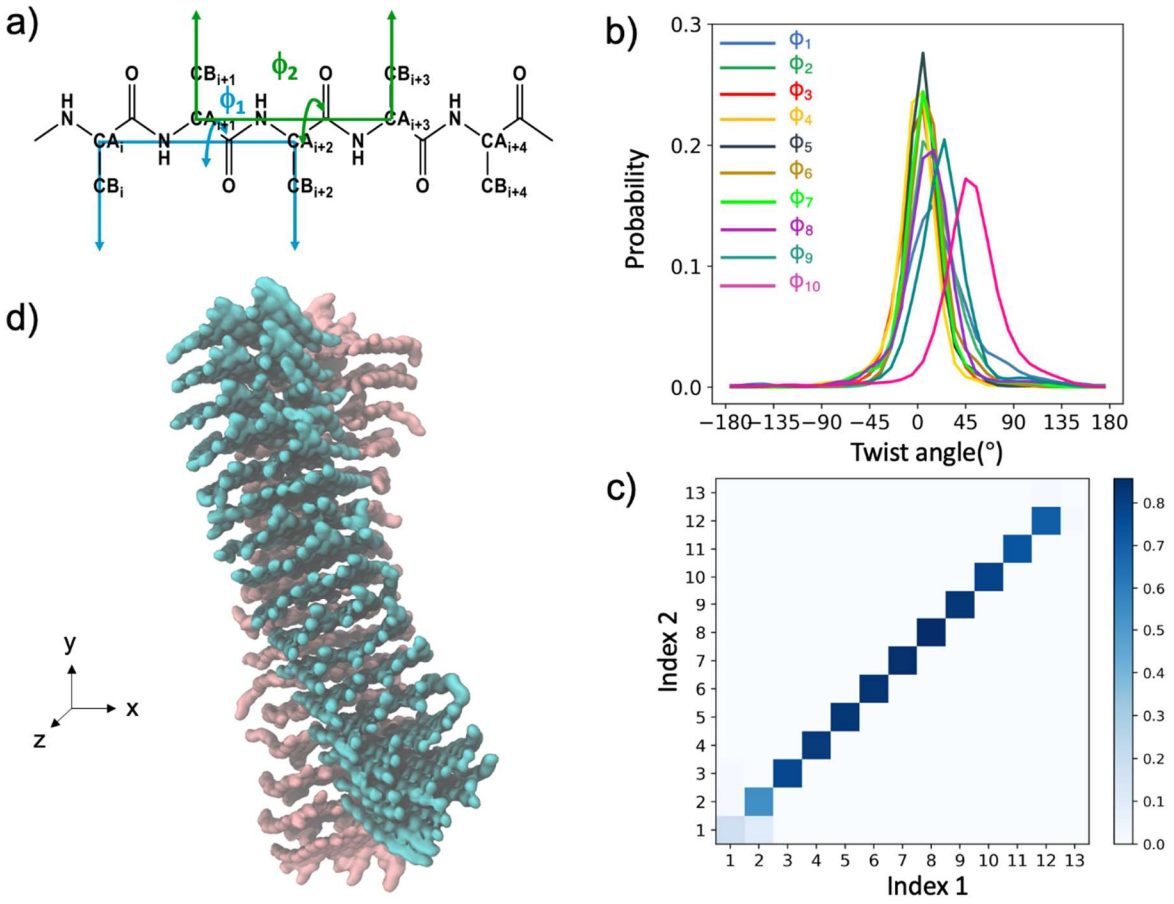

Figure 3. a) Definition of the twist angles ϕ (defined by the solid lines, dihedral angle $C\beta_i$-$C\alpha_i$-$C\alpha_{i+2}$-$C\beta_{i+2}$), where a positive angle represents right-handed twist, and a negative angle represents left-handed twist. b) Distributions of the averaged twist angle within each PA3 monomer. c) Backbone's 2D HB contact map for the PA3 ribbon, see method in SI for details. Here we show the results for the 8*16 PA system. d) Snapshot of backbone arrangement of PA3 ribbons where the y axis is the ribbon growth direction. Upper and lower parts of bilayer ribbons are shown in cyan and pink colors, respectively. Sidechains, lipid tail, ions and water are omitted for clarity.

Since previous studies have shown that PA3 tends to form a mixture of cylinders and narrow ribbons[3], it would be intriguing to figure out the structural difference between cylinder and ribbon structures. To do this, we constructed a cylindrical micelle structure with the same number of monomers as the ribbon structure (Figure S9b). Although the calculation of free energy differences between ribbon and cylinder is very difficult, we sought to gain insights by studying noncovalent interactions. Figure S9c-e and Figure S10 show that twisted ribbons tend to have a higher *β*-sheet content and hydrophobic collapse, while maintaining a low degree of

accessibility to solvent. From the geometry perspective, the fiber's radial stacking will cause dispersed stacking and lower β-sheet content for regions away from core. Therefore, it would be difficult for us to observe a morphology transition from narrow ribbons to cylinder through unbiased MD simulation. A hierarchical model developed by Nyrkova and co-workers[37] suggested that as the concentration increases, twisted ribbons will further stack into fibril and fiber structures. Another possible explanation would be that the cylindrical structure of PA3 observed by Moyer was produced under neutral conditions, and ours involves acidic pH, leading to a difference in the degree of protonation. To study this issue, we simulated a PA3 ribbon under neutral pH and we observed a torsion angle around -75º. This corresponds to a pitch ~38nm (Figure S11), which is much lower than the PA3 ribbon under acid pH (~135nm). A similar behavior in which twisted nanoribbons transform to cylinders as charge repulsion is increased has been previously reported for some PA assemblies[5,10,15]. Consequently, we have reasons to believe that the twisted ribbon structure observed in our simulations for low pH is a reasonable structure and our analysis suggests that right-handed twisted β-sheets originate from the right-handed twist nature of the strands within the peptide. This still requires synergy involving inter-strand hydrogen bond interactions. Further, the right-handed twisted β-sheets pack as left-handed structures along ribbon growth direction to form an overall left-handed twisted ribbon. We point out here that inter-strand Hbonding is known to be parallel to the fiber axis in cylindrical nanofibers[38–40]. However, our simulations indicate that the inter-strand Hbonding is perpendicular to the length axis in a ribbon-like assembly. Since the twisted ribbon assemblies here are very short given limitations on the size and time scale of simulations, it is possible that PA twisted ribbons transition into Hbonding parallel to the fiber axis or exhibit a combination of parallel and perpendicular bonding as they lengthen extensively to become highly one-dimensional. The inter-strand hydrogen bonding perpendicular to the elongation axis may only dominate in short fibers when nucleation and growth begins but a transition to both parallel and perpendicular will set in as long fibers grow past nucleation. Earlier work on supramolecular polymers indicates that strong interactions among monomers favor the formation of high molar mass one-dimensional assemblies[8,41].

The RGD epitope has been widely introduced into the terminus of the peptides to form biologically active nanostructures. For the present study, we are interested in the fact that the sequence PA4 ($C_{16}(VE)_2GRGD$, Figure S1) was found to form twisted ribbons[4,11]. To understand

GRGD's role in twisting the ribbons, we further simulated the PA4 ribbons. Starting from a flat ribbon, different degrees of torsion can be observed upon varying the width/length ratio (Figure S12). Surprisingly, unlike the previously observed left-handed twisted ribbon in PA3, PA4 tends to form a right-handed ribbon, and the torsion angle increases as the width/length ratio decreases (Figure 4a and Figure S12). Hence, our simulation can accurately capture the experimentally observed torsion property of PA4. Here we should note that in Cui's work[4], it was stated that the twisted ribbon formed by PA4 is left-handed, rather than the right-handed result we find. Their assignment was based on the intrinsic L-chirality of the amino acids and a TEM examination. However, it's difficult to distinguish the handedness of the nanostructures simply from cryo-TEM images; further stain and marks are needed to accurately determine the chirality[42]. Many previous works have also shown that even with natural amino acids (L-chirality), peptides can still form right-handed self-assembled structures[5,7,43]. Meanwhile, in the TEM image provided by Cui et al.[4,11], it appears that there are some right-handed twisted ribbons (Figure S13). In addition, related works have shown that positively charged amino groups, especially those located in the terminal region, tend to inhibit the right-handed β-sheets due to the positive charge[44,45]. Therefore, we believe that the right-handed ribbon found in our simulation is reasonable.

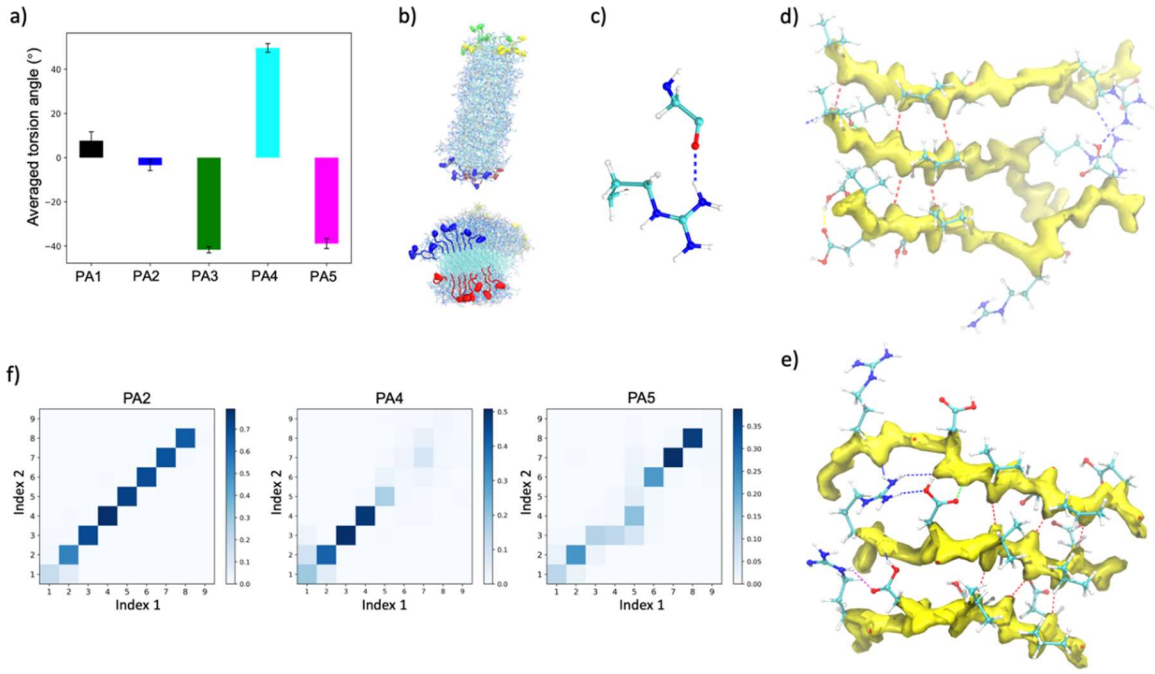

Figure 4. a) Averaged torsion angle of PA ribbons (PA1-PA5). All ribbons share the same width/length ratio, that is 8 layers in width and 16 layers in length. b) Top and side view of final simulation structures of PA4. c) Representative in-plane HB geometry between Arg sidechain and other hydrogen-acceptor group. Representative structure of PA4(d) and PA5(e) containing HBs. HB between backbones is shown in red dotted lines while HB between sidechain of protonated arginine and others is shown in blue dotted lines. f) Backbone's 2D HB contact map for PA2, PA4 and PA5 ribbons, which is calculated between two neighboring peptides.

C_{16}GRGD$(VE)_2$ (PA5) were also simulated to further explain the right-handedness of PA4 ribbons. We found that only PA4 ribbons possess a right-handed chirality, all other PAs tend to form a left-handed twisted ribbon (Figure 4a). The major difference between the VEVE and GRGD sequence is that Arg is positively charged and Gly is the only one achiral amino acid because it has no side chain[46]. On the one hand, electrostatic repulsions between Arg residues would break the backbone arrangement, thus weakening the β-sheet strength between neighboring monomers (Figure 4f). On the other hand, due to the strong HB formation tendency of the positively charged side chain of Arg[47,48], neighboring monomers can be stabilized, especially for PA5 (Figure 4d-e, Figure S15c), but the in-plane geometry (Figure 4c)[49] would break HBs between backbones (Figure 4f). So, when GRGD is located in the inner region of the peptide sequence, the dual lock effect of the hydrophobic lipid tail and VEVE hydrogen bond makes GRGD have little effect on the right-handed β-sheet. Conversely, when GRGD is after the VEVE sequence, PA4 not only loses its dual block effect, but also increases the solvent accessibility of head group (Figure S15a-b), which leads to a relatively weak inter-strand H-bonding. Meanwhile, in the previous section we discussed the twist of individual PA strand and concluded that the overall right-handed twist of the peptide is more strongly determined by the chirality of head group. Here by calculating the twist angle of the intrastrands, we found that PA4 loses its chirality, especially in the head region (Figure S7, S14b) while PA5 still maintains a right-hand twist for the head region (Figure S14c). Taken together, when GRGD is located in the head region coupled with a relatively weak β-sheet region, twisting chirality can be reversed. We believe that when the HB strength between the backbone is high enough, GRGD won't be able to change the chirality, but still weakens the degree of left-handedness. This hypothesis was confirmed by our simulation results for PA6 ($C_{16}(VE)_6$GRGD, Figure S16). Moreover, when we calculated the twist angles between neighboring strands, only PA4 shows a decrease in twist along the sequence while the others show the opposite trend (Figure S17). This also indicates why PA4 has the opposite handedness.

To further validate our thoughts above, we performed a conformationally constrained simulation on PA4 in which constraints were applied to maintain all the PA4s in an extended β-sheet geometry. Strikingly, when the PA4s are constrained, the ribbon changes from right-handed twist ($\Upsilon \approx 50^{o}$) to flat ($\Upsilon \approx 1^{o}$) (Figure S16a), and the β-sheet content is increased from 20% to 60% (Figure S18b), almost catching up with the β-sheet content in PA2 (Figure S5a). In general, our simulation results suggest that the incorporation of protonated Arg and achiral Gly do not have a bias toward right-handed β-sheets[34,44]. When the RGD epitope is introduced into the terminus of the PAs, it can destroy the right-handedness of the head group, breaking the inter-strand H-bonding between the backbone chains, therefore weakening the left-handed chirality of the nanostructures, and even reversing the left-handed chirality in some cases.

Chirality research related to β-sheet structure has always been under the spotlight and is of vital importance. In this paper, we conducted a systematic computational study based on hydrophobic-hydrophilic alternating motif molecules to identify the determining factors controlling the early stage of morphology and chiral properties of 1D ribbons composed of peptide amphiphiles. Our computational observations agreed well with previous experimental observations that flat ribbons tend to twist as the VE sequence length increases. Our results demonstrate that the right-handed character of the β-sheet originates from the right-handed twisted property of the strand itself, and is further stabilized by the hydrogen bonding between interstrands. The right-handed twisted β-sheets are found to stack along the growth direction in a left-handed manner, which leads to a left-handed twisted ribbon. Furthermore, a chirality change from left-handed to right-handed twisted ribbons can be observed by introducing GRGD to the head group, which implies that when achiral Gly and protonated Arg are located in the head region, they tend to not have the bias toward right-handed twisted β-sheets. The findings above may provide additional crucial details for a more precise design of chiral morphologies.

ASSOCIATED CONTENT

Supporting Information

The Supporting Information is available free of charge at XXXXX.

Details of the computation method are provided including models and simulation set up, and calculation methods (the analysis of secondary structure, the calculation of non-covalent

interactions, the definition of backbone's hydrogen bond 2D contact map, the description of conformationally constrained simulations). Additional tables (Tables S1−2) and figures (S1−S19) are included as mentioned in the text.

AUTHOR INFORMATION

Corresponding Author

George C. Schatz − *Department of Chemistry, Northwestern University, Evanston, Illinois 60208-3113, United States*; orcid.org/0000-0001-5837-4740

*E-mail: g-schatz@northwestern.edu.

Authors

Qinsi Xiong− *Department of Chemistry, Northwestern University, Evanston, Illinois 60208-3113, United States*; orcid.org/0000-0002-7511-0824

Samuel I. Stupp − *Department of Chemistry, Center for BioInspired Energy Science, and Department of Biomedical Engineering, Northwestern University, Evanston, Illinois 60208, United States; Department of Materials Science and Engineering, Northwestern University, Evanston, Illinois 60208, United States; Department of Medicine, Northwestern University, Chicago, Illinois 60611, United States; Simpson Querrey Institute for BioNanotechnology, Northwestern University, Chicago, Illinois 60611, United States*; orcid.org/0000-0002-5491-7442

Notes

The author declares no competing financial interest.

ACKNOWLEDGMENT

This work was supported by the Center for Bio-Inspired Energy Science (CBES), an Energy Frontier Research Center funded by the U.S. Department of Energy (DOE) Office of Basic Energy Sciences (DE-SC0000989).

REFERENCES

(1) Levin, A.; Hakala, T. A.; Schnaider, L.; Bernardes, G. J. L.; Gazit, E.; Knowles, T. P. J. Biomimetic Peptide Self-Assembly for Functional Materials. *Nat. Rev. Chem.* **2020**, *4*, 615–634.

(2) Yuan, C.; Ji, W.; Xing, R.; Li, J.; Gazit, E.; Yan, X. Hierarchically Oriented Organization in Supramolecular Peptide Crystals. *Nat. Rev. Chem.* **2019**, 3, 567–588.

(3) Cui, H.; Muraoka, T.; Cheetham, A. G.; Stupp, S. I. Self-Assembly of Giant Peptide Nanobelts. *Nano Lett.* **2009**, *9*, 945–951.

(4) Moyer, T. J.; Cui, H.; Stupp, S. I. Tuning Nanostructure Dimensions with Supramolecular Twisting. *J. Phys. Chem. B* **2013**, *117*, 4604–4610.

(5) Sangji, M. H.; Sai, H.; Chin, S. M.; Lee, S. R.; Sasselli, I. R.; Palmer, L. C.; Stupp, S. I. Supramolecular Interactions and Morphology of Self-Assembling Peptide Amphiphile Nanostructures. *Nano Lett.* **2021**, *21*, 6146–6155.

(6) Sato, K.; Ji, W.; Álvarez, Z.; Palmer, L. C.; Stupp, S. I. Chiral Recognition of Lipid Bilayer Membranes by Supramolecular Assemblies of Peptide Amphiphiles. *ACS Biomater. Sci. Eng.* **2019**, *5*, 2786–2792.

(7) Pashuck, E. T.; Stupp, S. I. Direct Observation of Morphological Tranformation from Twisted Ribbons into Helical Ribbons. *J. Am. Chem. Soc.* **2010**, *132*, 8819–8821.

(8) Tantakitti, F.; Boekhoven, J.; Wang, X.; Kazantsev, R. V.; Yu, T.; Li, J.; Zhuang, E.; Zandi, R.; Ortony, J. H.; Newcomb, C. J.; *et al.* Energy Landscapes and Functions of Supramolecular Systems. *Nat. Mater.* **2016**, *15*, 469–476.

(9) Hartgerink, J. D.; Beniash, E.; Stupp, S. I. Self-Assembly and Mineralization of Peptide-Amphiphile Nanofibers. *Science* **2001**, *294*, 1684–1688.

(10) Gao, C.; Li, H.; Li, Y.; Kewalramani, S.; Palmer, L. C.; Dravid, V. P.; Stupp, S. I.; Cruz, M. O. de la; Bedzyk, M. J. Electrostatic Control of Polymorphism in Charged Amphiphile Assemblies. *J. Phys. Chem. B* **2017**, *121*, 1623–1628.

(11) Cui, H.; Cheetham, A. G.; Pashuck, E. T.; Stupp, S. I. Amino Acid Sequence in Constitutionally Isomeric Tetrapeptide Amphiphiles Dictates Architecture of One-Dimensional Nanostructures. *J. Am. Chem. Soc.* **2014**, *136*, 12461–12468.

(12) Hendricks, M. P.; Sato, K.; Palmer, L. C.; Stupp, S. I. Supramolecular Assembly of Peptide Amphiphiles. *Acc. Chem. Res.* **2017**, *50*, 2440–2448.

(13) Zhao, Y.; Deng, L.; Yang, W.; Wang, D.; Pambou, E.; Lu, Z.; Li, Z.; Wang, J.; King, S.; Rogers, S.; et al. Tuning One-Dimensional Nanostructures of Bola-Like Peptide Amphiphiles by Varying the Hydrophilic Amino Acids. *Chem. - Eur. J.* **2016**, *22*, 11394–11404.

(14) Fishwick, C. W. G.; Beevers, A. J.; Carrick, L. M.; Whitehouse, C. D.; Aggeli, A.; Boden, N. Structures of Helical β-Tapes and Twisted Ribbons: The Role of Side-Chain Interactions on Twist and Bend Behavior. *Nano Lett.* **2003**, *3*, 1475–1479.

(15) Hu, Y.; Lin, R.; Zhang, P.; Fern, J.; Cheetham, A. G.; Patel, K.; Schulman, R.; Kan, C.; Cui, H. Electrostatic-Driven Lamination and Untwisting of β-Sheet Assemblies. *ACS Nano* **2016**, *10*, 880–888.

(16) Zaldivar, G.; Conda-Sheridan, M.; Tagliazucchi, M. Twisting of Charged Nanoribbons to

Helicoids Driven by Electrostatics. *J. Phys. Chem. B* **2020**, *124*, 3221–3227.

(17) Frederix, P. W. J. M.; Patmanidis, I.; Marrink, S. J. Molecular Simulations of Self-Assembling Bio-Inspired Supramolecular Systems and Their Connection to Experiments. *Chem. Soc. Rev.* **2018**, *47*, 3470–3489.

(18) Manandhar, A.; Kang, M.; Chakraborty, K.; Tang, P. K.; Loverde, S. M. Molecular Simulations of Peptide Amphiphiles. *Org. Biomol. Chem.* **2017**, *15*, 7993–8005.

(19) Lee, O.-S.; Stupp, S. I.; Schatz, G. C. Atomistic Molecular Dynamics Simulations of Peptide Amphiphile Self-Assembly into Cylindrical Nanofibers. *J. Am. Chem. Soc.* **2011**, *133*, 3677–3683.

(20) Lee, O.-S.; Cho, V.; Schatz, G. C. Modeling the Self-Assembly of Peptide Amphiphiles into Fibers Using Coarse-Grained Molecular Dynamics. *Nano Lett.* **2012**, *12*, 4907–4913.

(21) Fu, I. W.; Nguyen, H. D. Sequence-Dependent Structural Stability of Self-Assembled Cylindrical Nanofibers by Peptide Amphiphiles. *Biomacromolecules* **2015**, *16*, 2209–2219.

(22) Lai, C. T.; Rosi, N. L.; Schatz, G. C. All-Atom Molecular Dynamics Simulations of Peptide Amphiphile Assemblies That Spontaneously Form Twisted and Helical Ribbon Structures. *J. Phys. Chem. Lett.* **2017**, *8*, 2170–2174.

(23) Sunde, M.; Serpell, L. C.; Bartlam, M.; Fraser, P. E.; Pepys, M. B.; Blake, C. C. F. Common Core Structure of Amyloid Fibrils by Synchrotron X-Ray Diffraction. *J. Mol. Biol.* **1997**, *273*, 729–739.

(24) Makin, O. S.; Atkins, E.; Sikorski, P.; Johansson, J.; Serpell, L. C. Molecular Basis for Amyloid Fibril Formation and Stability. *Proc. Natl. Acad. Sci. U. S. A.* **2005**, *102*, 315–320.

(25) Eisenberg, D.; Jucker, M. The Amyloid State of Proteins in Human Diseases. *Cell* **2012**, *148*, 1188–1203.

(26) Lamm, M. S.; Rajagopal, K.; Schneider, J. P.; Pochan, D. J. Laminated Morphology of Nontwisting β-Sheet Fibrils Constructed via Peptide Self-Assembly. *J. Am. Chem. Soc.* **2005**, *127*, 16692–16700.

(27) Brack, A.; Orgel, L. E. β Structures of Alternating Polypeptides and Their Possible Prebiotic Significance. *Nature* **1975**, *256*, 383–387.

(28) Schneider, J. P.; Pochan, D. J.; Ozbas, B.; Rajagopal, K.; Pakstis, L.; Kretsinger, J. Responsive Hydrogels from the Intramolecular Folding and Self-Assembly of a Designed Peptide. *J. Am. Chem. Soc.* **2002**, *124*, 15030–15037.

(29) Rodriguez, L. M. D. L.; Yacine Hemar; Jillian Cornish; A. Brimble, M. Structure–Mechanical Property Correlations of Hydrogel Forming β-Sheet Peptides. *Chem. Soc. Rev.* **2016**, *45*, 4797–4824.

(30) Shamovsky, I. L.; Ross, G. M.; Riopelle, R. J. Theoretical Studies on the Origin of β-Sheet Twisting. *J. Phys. Chem. B* **2000**, *104*, 11296–11307.

(31) Chothia, C. Conformation of Twisted β-Pleated Sheets in Proteins. *J.Mol. Biol.* **1973**, *75*, 295–302.

(32) Bour, P.; Keiderling, T. A. Structure, Spectra and the Effects of Twisting of β-Sheet Peptides. A Density Functional Theory Study. *J. Mol. Struct.: THEOCHEM* **2004**, *675*, 95–105.

(33) Wang, M.; Zhou, P.; Wang, J.; Zhao, Y.; Ma, H.; Lu, J. R.; Xu, H. Left or Right: How Does Amino Acid Chirality Affect the Handedness of Nanostructures Self-Assembled from Short Amphiphilic Peptides? *J. Am. Chem. Soc.* **2017**, *139*, 4185–4194.

(34) Wang, M.; Zhao, Y.; Zhang, L.; Deng, J.; Qi, K.; Zhou, P.; Ma, X.; Wang, D.; Li, Z.; Wang, J.; et al. Unexpected Role of Achiral Glycine in Determining the Suprastructural Handedness of Peptide Nanofibrils. *ACS Nano* **2021**, *15*, 10328–10341.

(35) Wadai, H.; Yamaguchi, K.; Takahashi, S.; Kanno, T.; Kawai, T.; Naiki, H.; Goto, Y. Stereospecific Amyloid-like Fibril Formation by a Peptide Fragment of B2-Microglobulin. *Biochemistry* **2005**, *44*, 157–164.

(36) Lara, C.; Reynolds, N. P.; Berryman, J. T.; Xu, A.; Zhang, A.; Mezzenga, R. ILQINS Hexapeptide, Identified in Lysozyme Left-Handed Helical Ribbons and Nanotubes, Forms Right-Handed Helical Ribbons and Crystals. *J. Am. Chem. Soc.* **2014**, *136*, 4732–4739.

(37) Aggeli, A.; Nyrkova, I. A.; Bell, M.; Harding, R.; Carrick, L.; McLeish, T. C. B.; Semenov, A. N.; Boden, N. Hierarchical Self-Assembly of Chiral Rod-like Molecules as a Model for Peptide β-Sheet Tapes, Ribbons, Fibrils, and Fibers. *Proc. Natl. Acad. Sci. U. S. A.* **2001**, *98*, 11857–11862.

(38) Velichko Y. S.; Stupp, S. I.; Cruz, M. O. de la. Molecular Simulation Study of Peptide Amphiphile Self-Assembly. *J. Phys. Chem. B* **2008**, *112*, 2326–2334.

(39) Paramonov, S. E.; Jun, H.; Hartgerink, J. D. Self-Assembly of Peptide−Amphiphile Nanofibers: The Roles of Hydrogen Bonding and Amphiphilic Packing. *J. Am. Chem. Soc.* **2006**, *128*, 7291–7298.

(40) Jiang, H.; Guler, M. O.; Stupp, S. I. The Internal Structure of Self-Assembled Peptide Amphiphiles Nanofibers. *Soft Matter* **2007**, *3*, 454–462.

(41) Sijbesma, R. P.; Beijer, F. H.; Brunsveld, L.; Folmer, B. J. B.; Hirschberg, J. H. K. K.; Lange, R. F. M.; Lowe, J. K. L.; Meijer, E. W. Reversible Polymers Formed from Self-Complementary Monomers Using Quadruple Hydrogen Bonding. *Science* **1997**, *278*, 1601–1604.

(42) Lin, Y.-A.; Ou, Y.-C.; Cheetham, A. G.; Cui, H. Supramolecular Polymers Formed by ABC Miktoarm Star Peptides. *ACS Macro Lett.* **2013**, *2*, 1088–1094.

(43) Stupp, S. I.; Palmer, L. C. Supramolecular Chemistry and Self-Assembly in Organic Materials Design. *Chem. Mater.* **2014**, *26*, 507–518.

(44) Fujiwara, K.; Ebisawa, S.; Watanabe, Y.; Toda, H.; Ikeguchi, M. Local Sequence of Protein β-Strands Influences Twist and Bend Angles. *Proteins* **2014**, *82*, 1484–1493.

(45) Xie, Y.; Wang, Y.; Qi, W.; Huang, R.; Su, R.; He, Z. Reconfigurable Chiral Self-Assembly of Peptides through Control of Terminal Charges. *Small* **2017**, *13*, 1700999.

(46) Wang, L.; O'Connell, T.; Tropsha, A.; Hermans, J. Molecular Simulations of β-Sheet Twisting. *J. Mol. Biol.* **1996**, *262*, 283–293.

(47) Nie, B.; Stutzman, J.; Xie, A. A Vibrational Spectral Maker for Probing the Hydrogen-Bonding Status of Protonated Asp and Glu Residues. *Biophys. J.* **2005**, *88*, 2833–2847.

(48) Chan, A. W. E.; Laskowski, R. A.; Selwood, D. L. Chemical Fragments That Hydrogen Bond to Asp, Glu, Arg, and His Side Chains in Protein Binding Sites. *J. Med. Chem.* **2010**, *53*, 3086–3094.

(49) Armstrong, C. T.; Mason, P. E.; Anderson, J. L. R.; Dempsey, C. E. Arginine Side Chain Interactions and the Role of Arginine as a Gating Charge Carrier in Voltage Sensitive Ion Channels. *Sci. Rep.* **2016**, *6*, 21759.